Progress In Electromagnetics Research M, Vol. 74, 25–32, 2018

Nonlinear Single Negative Metamaterials Based on Varactor Diodes

Tuanhui Feng[1, 2, *], Hongpei Han[1], and Limin Wang[1]

Abstract—In this paper, the nonlinear single negative metamaterials (NLSNM) based on the microstrip loaded with varactor diodes are investigated. It is found that the NLSNM, including nonlinear epsilon-negative metamaterial (NLENM) and nonlinear mu-negative metamaterial (NLMNM) can be realized by loading varactor diodes and chip inductors onto the microstrip, and their transmission gaps can be controlled conveniently by the signal power. In addition, the nonlinear property of the heterostructure constructed of NLMNM and epsilon-negative metamaterial (ENM) is also studied, and the results show that the transmission property, especially the transmittance of the tunneling peak of the NLMNM-ENM heterostructure can also be regulated by the signal power. The NLSNM may have important potential applications in the microwave switch controlled by the signal power.

1. INTRODUCTION

Single negative metamaterials (SNM), as one kind of metamaterials, have been extensively investigated in the past few years, due to their unique electromagnetic properties and important applications [1–16]. There are two types of SNM: one is the epsilon-negative metamaterial (ENM), in which the permittivity is negative, but the permeability is positive; the other is the mu-negative metamaterial (MNM), in which the permeability is negative, but the permittivity is positive. The isolated ENM or MNM is opaque and supports only evanescent waves, but many composite structures constructed of the ENM and the MNM can be transparent to electromagnetic waves and possess some extraordinary electromagnetic properties and important applications [1–8]. For instance, electromagnetic waves can tunnel through a matched ENM-MNM heterostructure, and a subwavelength resonator can be realized based on the ENM-MNM heterostructure [1–3]. The sandwich structure constructed of ENM, MNM and air can also be transparent to electromagnetic waves, and new wireless information and energy transfer system can be realized based on the ENM-Air-MNM structure [4]. The photonic spin Hall effect insensitive to interface fluctuations was observed in the waveguide composed of two types of SNM, and it may be useful to the manipulation of electromagnetic signals [5]. In addition, the sole ENM or MNM also has some important applications. For example, the ultra-small single negative metamaterial insulator for mutual coupling reduction of the high-profile monopole antenna array was proposed in [6]. In order to implement the SNM, a lot of structures have been presented [2, 3, 9–13], such as the array of split ring resonators or thin metal wires [9, 10], the transmission lines with lumped capacitors and inductors loading and those with split ring resonators or complementary split ring resonators loading [2, 3, 11, 12].

In addition, the investigations on nonlinear metamaterials have also aroused great interests of many researchers in the last decade to explore the extraordinary nonlinear properties of the metamaterials [17–26]. In [17–23], the authors indicated that the nonlinear metamaterials could be realized by introducing the nonlinear elements of varactor diodes in the building blocks of the metamaterials. In this paper, the nonlinear single negative metamaterials (NLSNM) based on the microstrip loaded with varactor diodes

Received 18 July 2018, Accepted 21 September 2018, Scheduled 3 October 2018

* Corresponding author: Tuanhui Feng (tuanhuifeng@xcu.edu.cn).

[1] School of Electrical Engineering, Xuchang University, Xuchang 461000, China. [2] Key Laboratory of Advanced Micro-structure Materials, MOE, School of Physics Science and Engineering, Tongji University, Shanghai 200092, China.

are proposed. Firstly, the NLSNM, including the nonlinear epsilon-negative metamaterial (NLENM) and nonlinear mu-negative metamaterial (NLMNM) are realized by loading varactor diodes and chip inductors onto the microstrip and their nonlinear properties investigated. In addition, in order to further confirm the single negative property of the NLSNM and meanwhile explore their applications, the heterostructure constructed of the NLMNM and ENM is fabricated, and its nonlinear properties are measured and analyzed.

2. NLSNM BASED ON VARACTOR DIODES

As shown in Figure 1(a), the NLSNM are fabricated by periodically loading varactor diodes and chip inductors onto the microstrip. Each unit consists of two varactor diodes and one chip inductor with the same unit length of $d = 12\,\text{mm}$. When loading the varactor diodes, the double gaps are periodically sculptured on the strip of the microstrip, and the varactor diodes are soldered onto the microstrip crossing the gaps. All the varactor diodes are connected end to end or head to head. For loading the chip inductors, the periodic through-holes are introduced in the microstrip, and the chip inductors are embedded into the through-holes by soldering tin. The schematic and circuit model of each unit of the NLSNM is given in Figure 1(c). In our experiments the substrate of the microstrip is F4B with relative permittivity of 2.65, thickness of 1.0 mm and loss tangent of 0.001. The strip width of microstrip is designed to be 2.73 mm to match the characteristic impedance 50 Ω. For these parameters, the distributed parameters of the microstrip are $L_0 = 248\,\text{nH/m}$ and $C_0 = 99\,\text{pF/m}$, respectively. In addition, the varactor diodes of infineon BBY52 are employed for all our samples.

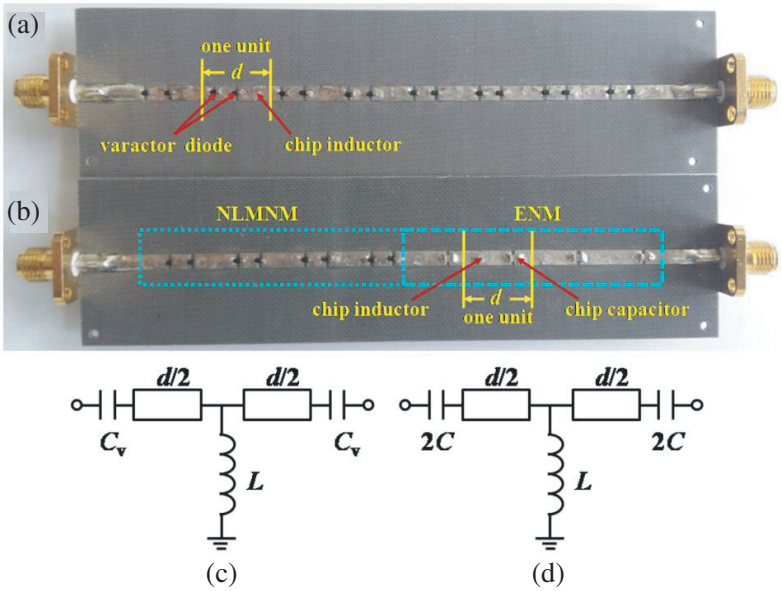

Figure 1. (a) The photograph of the NLSNM. (b) The photograph of the NLMNM-ENM hetorostructure. (c) The schematic and circuit model of each unit of the NSNM with the loading varactor diodes (C_v) and chip inductors (L). (d) The schematic and circuit model of each unit of the ENM with the loading chip capacitors (C) and chip inductors (L).

When the value of the loaded chip inductors is chosen to be $L = 4.7\,\text{nH}$, the transmission curves (indicated by the amplitude of the transmission coefficient, $|S_{21}|$) of the structure shown in Figure 1(a) under different signal powers are measured by employing the sole Agilent N5242A Vector Network Analyzer and shown in Figure 2(a). From Figure 2(a) one can see that the transmission gaps can be controlled conveniently by the signal power, and the gap width and depth increase gradually with the enhancement of the signal power. When the signal power is 0 dBm, there is no transmission gap, and when the signal power is increased to 17 dBm, the gap is as wide as 0.98 GHz and as deep as

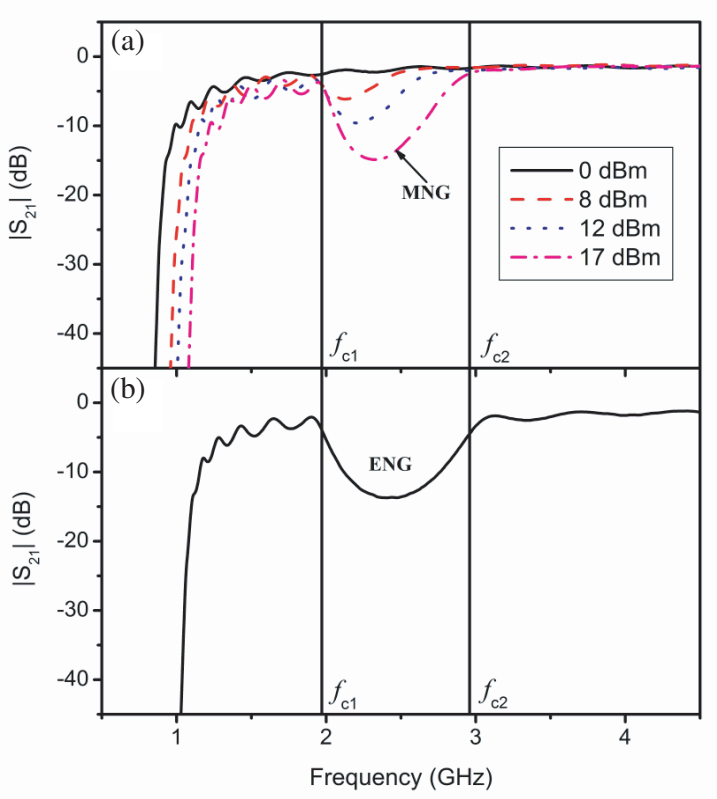

Figure 2. The transmission curves of (a) the structure shown in Figure 1(a) under different signal powers when the value of the loaded chip inductors is $L = 4.7\,\text{nH}$ and (b) the microstrip metamaterial in the right half of the heterostructure shown in Figure 1(b).

$-16\,\text{dB}$. According to the dispersion relation determined by periodic analysis, the effective permittivity and permeability of the microstrip metamaterial shown in Figure 1(a) can be given by the following approximate expressions [27]:

$$\varepsilon_{eff} \approx \left(C_0 - 1/\omega^2 Ld\right)/p, \tag{1}$$

$$\mu_{eff} \approx p\left(L_0 - 2/\omega^2 Cd\right), \tag{2}$$

where p is the structure constant of the microstrip (in our experiment, its value is 5.04); d is the unit length of the microstrip metamaterial; C and L are the values of the loaded varactor diodes and chip inductors, respectively; C_0 and L_0 are the distributed parameters of the microstrip. When the signal power is 17 dBm, the capacitance of the varactor diodes is about 1.8 pF, and under this case, the effective permittivity and permeability of the microstrip metamaterial shown in Figure 1(a) are calculated according to Eqs. (1) and (2) and depicted in Figure 3. In Figure 3, as shown by the arrows, the black solid line indicates the change of the effective permittivity with the frequency, and the red dashed line presents the effective permeability. From Figure 3, it can be seen that the microstrip metamaterial has $\mu_{eff} < 0$ and $\varepsilon_{eff} > 0$ in the frequency range from $f_{c1} = 2.12\,\text{GHz}$ to $f_{c2} = 3.08\,\text{GHz}$. So the corresponding transmission gap depicted by the magenta dashed dotted line in Figure 2(a) is the mu-negative gap (MNG), and the MNM is obtained in the frequency range between $f_{c1} = 1.97\,\text{GHz}$ and $f_{c2} = 2.95\,\text{GHz}$ by utilizing the structure shown in Figure 1(a). Comparing the values of f_{c1} and f_{c2} in Figure 2(a) with the calculated values shown in Figure 3, there exists a difference, which is mainly because Eqs. (1) and (2) are deduced based on the infinite periodic structure, and they are approximate. According to similar calculations, it can be known that in Figure 2(a) all the transmission gaps under other signal powers are MNGs. Therefore, when the value of the loaded chip inductors is chosen to be $L = 4.7\,\text{nH}$, the NLMNM can be realized using the structure shown in Figure 1(a). Moreover, as the MNG can be either closed or as deep as $-16\,\text{dB}$ (if the signal power continues to increase, the

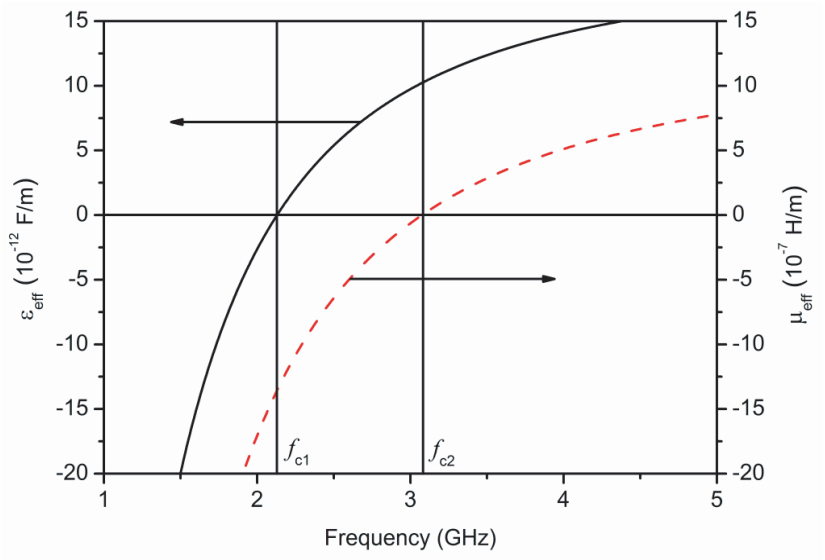

Figure 3. The calculated effective permittivity and permeability of the microstrip metamaterial shown in Figure 1(a) under the signal power of 17 dBm when the value of the loaded chip inductors is $L = 4.7$ nH.

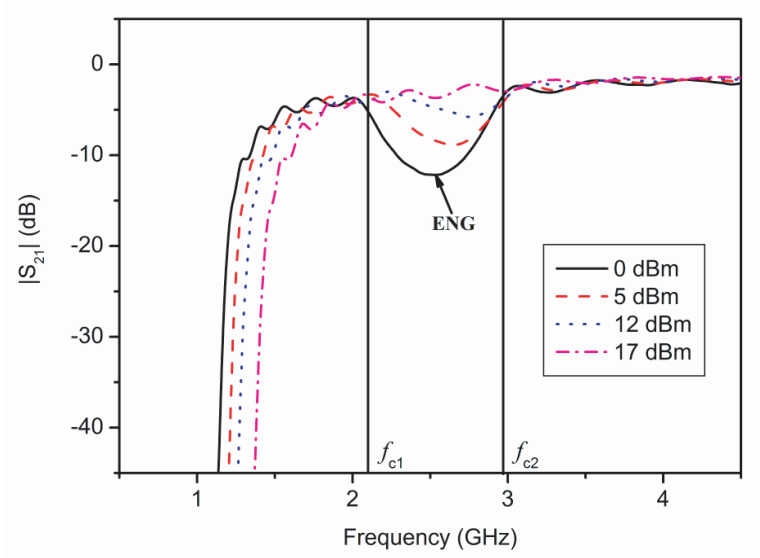

Figure 4. The transmission curves of the structure shown in Figure 1(a) under different signal powers when the value of the loaded chip inductors is $L = 2.2$ nH.

transmittance of the gap will become smaller), the NLMNM may be useful in the switching device controlled by the signal power in the microwave communication system.

To achieve the NLENM, the value of the loaded chip inductors is chosen to be $L = 2.2$ nH. Figure 4 shows the transmission curves of the microstrip metamaterial shown in Figure 1(a) under different signal powers in the case of $L = 2.2$ nH. It can be seen that the transmission gaps can also be controlled conveniently by the signal power, and the gap width and depth decrease gradually with the increase of the signal power. When the signal power is 0 dBm, the transmission gap is as wide as 0.88 GHz and as deep as -13 dB, and the gap is closed when the signal power is increased to 17 dBm. When the signal power is 0 dBm, the value of the varactor diodes is about 2.8 pF, and here the effective permittivity and permeability of the microstrip metamaterial shown in Figure 1(a) are calculated and depicted in

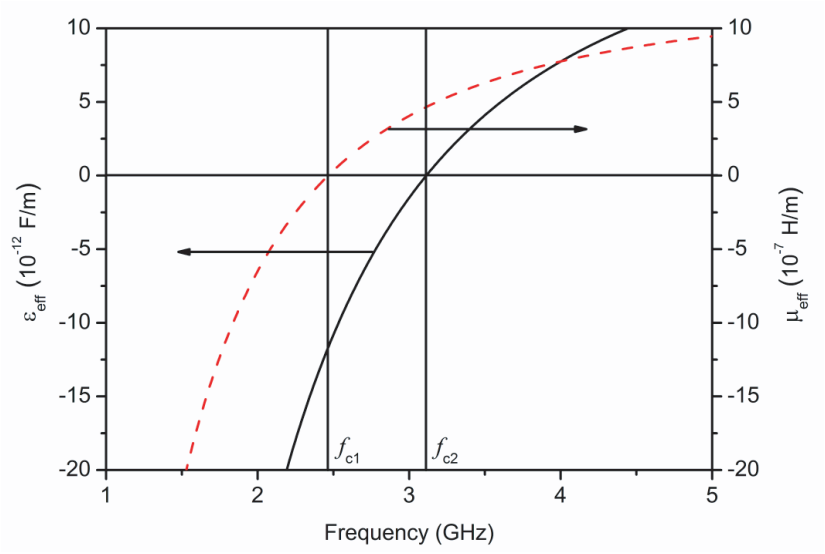

Figure 5. The calculated effective permittivity and permeability of the microstrip metamaterial shown in Figure 1(a) under the signal power of 0 dBm when the value of the loaded chip inductors is $L = 2.2$ nH.

Figure 5. From Figure 5, one can clearly see that the microstrip metamaterial has $\varepsilon_{eff} < 0$ and $\mu_{eff} > 0$ in the frequency range between $f_{c1} = 2.45$ GHz and $f_{c2} = 3.1$ GHz. So the corresponding transmission gap depicted by the black solid line in Figure 4 is the epsilon-negative gap (ENG), and the ENM is obtained in the frequency range between $f_{c1} = 2.09$ GHz and $f_{c2} = 2.97$ GHz. The differences between the calculation values and measurement values for f_{c1} and f_{c2} also mainly result from the approximate characteristic of Eqs. (1) and (2). Similarly, it can also be known that the transmission gaps under other signal powers are all ENGs in Figure 4. Therefore, the NLENM is acquired using the structure shown in Figure 1(a) when the value of the loaded chip inductors is chosen to be $L = 2.2$ nH. Obviously, the NLENM is also hopeful to be applied in the signal-controlled switching device.

3. NONLINEAR PROPERTIES OF THE NLMNM-ENM HETEROSTRUCTURE

In order to further confirm the single negative property of the NLSNM and meanwhile explore their applications, the heterostructure constructed of the NLMNM and ENM is fabricated, as shown in Figure 1(b). In Figure 1(b), The ENM is realized by periodically loading series chip capacitors and shunt chip inductors onto the microstrip. Each unit consists of one chip capacitor and one chip inductor with the same unit length of $d = 12$ mm. The schematic and circuit model of each unit of the ENM is given in Figure 1(d). For the NLMNM in the heterostructure, the loaded lumped elements are the same as that mentioned above, and for the ENM, the values of the loaded series capacitors and shunt inductors are $C = 1.6$ pF and $L = 2.2$ nH, respectively. Based on the dispersion relation determined by periodic analysis, the effective permittivity and permeability of the microstrip metamaterial in the right half of the heterostructure shown in Figure 1(b) can also be given by Eqs. (1) and (2), and here C denotes the value of the series chip capacitors. According to Eqs. (1) and (2), the effective permittivity and permeability of the microstrip metamaterial in the right half of the heterostructure shown in Figure 1(b) are calculated and shown in Figure 6. The transmission curve is measured and shown in Figure 2(b). From Figure 6 one can clearly see that the microstrip metamaterial has $\varepsilon_{eff} < 0$ and $\mu_{eff} > 0$ in the frequency range from $f_{c1} = 2.3$ GHz to $f_{c2} = 3.1$ GHz. So in Figure 2(b) the corresponding transmission gap is the ENG, and the ENM is obtained in the frequency range between $f_{c1} = 1.97$ GHz and $f_{c2} = 2.95$ GHz by using the microstrip metamaterial in the right half of the heterostructure shown in Figure 1(b). Here, there still exists a difference between the calculation values and measurement values for f_{c1} and f_{c2}, and it is also mainly because Eqs. (1) and (2) are approximate. Obviously, the frequency range of the ENM is the same as the NLMNM under the signal power of

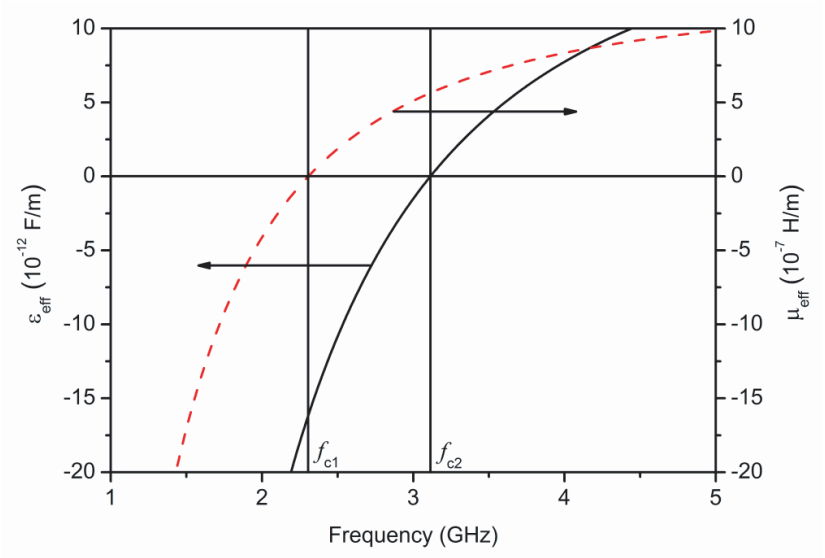

Figure 6. The calculated effective permittivity and permeability of the microstrip metamaterial in the right half of the heterostructure shown in Figure 1(b).

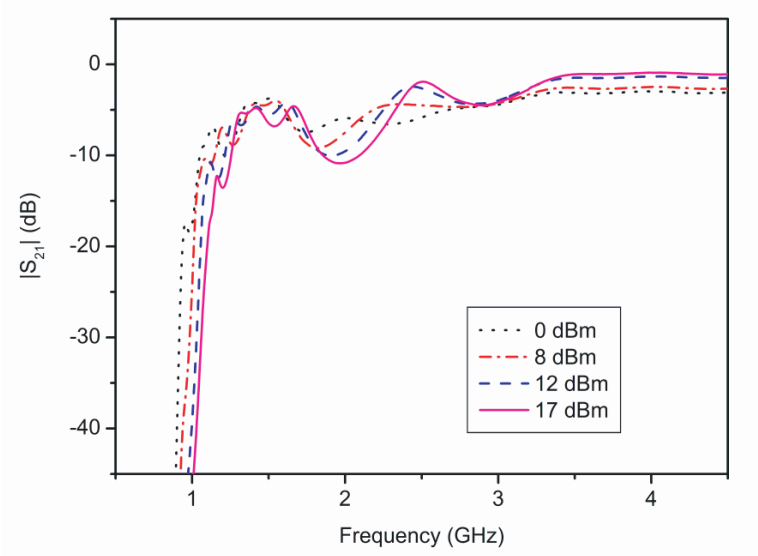

Figure 7. The transmission curves of the NLMNM-ENM heterostructure shown in Figure 1(b) under different signal powers.

17 dBm.

Figure 7 shows the transmission curves of the NLMNM-ENM heterostructure shown in Figure 1(b) under different signal powers. It is obvious that the signal power also has a great effect on the transmission property of the NLMNM-ENM hetorostructure. As well known, the complete electromagnetic tunneling only occurs in the MNM-ENM heterostructure when the average permittivity and average permeability are simultaneously zero [1–3]. In Figure 7, when the signal power is 0 dBm, there is no electromagnetic tunneling as here the nonlinear metamaterial in the left half of the heterostructure has no transmission gap, and the tunneling condition is not met. When the signal power is increased, as the MNG begins to appear for the nonlinear metamaterial in the left half of the heterostructure, and the MNM is obtained, the tunneling phenomenon begins to emerge in the heterostructure. When the signal power is increased to 17 dBm, the tunneling condition is best satisfied,

and the tunneling peak with a highest transmittance is obtained. The transmission properties of the NLMNM-ENM heterostructure confirm the mu-negative property of the NLMNM. Moreover, with these features, the NLMNM-ENM heterostructure may also have important applications in some practical signal-controlled microwave switches.

4. CONCLUSION

In conclusion, the NLSNM, including the NLENM and NLMNM, are realized by periodically loading varactor diodes and chip inductors onto the microstrip and their nonlinear properties measured. The results show that for the NLENM and NLMNM, the transmission gaps can be controlled conveniently by the signal power. For the NLMNM, the gap width and depth increase gradually with the enhancement of the signal power while they decrease gradually with the increase of the signal power for the NLENM. For two types of NLSNM, the single negative gaps can either be closed or have a certain depth along with different signal powers, which make them useful in the signal-controlled switching device. In addition, the nonlinear properties of the NLMNM-ENM heterostructure are also investigated, and the results show that the signal power also has a great effect on the electromagnetic tunneling in the NLMNM-ENM hetorostructure. When the signal power is small, there is no electromagnetic tunneling in the hetorostructure, and when the signal power is increased to a certain value, the tunneling peak with the highest transmittance can be obtained. With these properties, the NLMNM-ENM heterostructure may also be promising for being utilized in some practical signal-controlled microwave switches.

ACKNOWLEDGMENT

This work is supported by the National Natural Science Foundation of China (Grant No. U1504110), the Aid Project for the Leading Young Teachers in Henan Provincial Institutions of Higher Education (Grant No. 2014GGJS-117), the Natural Science Foundation of Henan Province of China (Grant Nos. 182300410199, 162300410237) and the Development Project for Science & Technology of Henan Province of China (Grant Nos. 182102210509, 172102210470).

REFERENCES

1. Alù, A. and N. Engheta, "Pairing an epsilon-negative slab with a mu-negative slab: Resonance, tunneling and transparency," *IEEE Trans. Antennas Propagat.*, Vol. 51, 2558–2571, 2003.
2. Fujishige, T., C. Caloz, and T. Itoh, "Experimental demonstration of transparency in the ENG-MNG pair in a CRLH transmission-line implementation," *Microw. Opt. Tech. Lett.*, Vol. 46, 476–481, 2005.
3. Feng, T. H., Y. H. Li, J. Y. Guo, L. He, H. Q. Li, Y. W. Zhang, Y. L. Shi, and H. Chen, "Highly localized mode in a structure made of epsilon-negative and mu-negative metamaterial," *J. Appl. Phys.*, Vol. 104, 013107, 2008.
4. Feng, T. H., Y. H. Li, H. T. Jiang, Y. Sun, L. He, H. Q. Li, Y. W. Zhang, Y. L. Shi, and H. Chen, "Electromagnetic tunneling in a sandwich structure containing single negative media," *Phys. Rev. E*, Vol. 79, 026601, 2009.
5. Guo, Z. W., H. T. Jiang, Y. Long, K. Yu, J. Ren, C. H. Xue, and H. Chen, "Photonic spin Hall effect in waveguides composed of two types of single-negative metamaterials," *Scientific Reports*, Vol. 7, 7724, 2017.
6. Qiu, Y., L. Peng, X. Jiang, Z. Sun, and S. Tang, "Ultra-small single-negative metamaterial insulator for mutual coupling reduction of high-profile monopole antenna array," *Progress In Electromagnetics Research C*, Vol. 72, 197–205, 2017.
7. Chen, Y. H., "Defect modes merging in one-dimensional photonic crystals with multiple single-negative material defects," *Appl. Phys. Lett.*, Vol. 92, 011925, 2008.
8. Feng, T. H., F. Yang, Y. H. Li, Y. Sun, H. Lu, H. T. Jiang, Y. W. Zhang, and H. Chen, "Light tunneling effect tuned by a meta-interface with electromagnetically-induced-transparency-like properties," *Appl. Phys. Lett.*, Vol. 102, 251908, 2013.

9. Pendry, J. B., A. J. Holden, W. J. Stewart, and I. Youngs, "Extremely low frequency plasmons in metallic mesostructures," *Phys. Rev. Lett.*, Vol. 76, 4773–4776, 1996.
10. Pendry, J. B., A. J. Holden, D. J. Robbins, and W. J. Stewart, "Magnetism from conductors and enhanced nonlinear phenomena," *IEEE Trans. Microw. Theory Tech.*, Vol. 47, No. 11, 2075–2084, 1999.
11. Martin, F., J. Bonache, F. Falcone, M. Sorolla, and R. Marques, "Split ring resonator-based left-handed coplanar waveguide," *Appl. Phys. Lett.*, Vol. 83, 4652–4654, 2003.
12. Falcone, F., T. Lopetegi, M. A. G. Laso, J. D. Baena, J. Bonache, M. Beruete, R. Marqués, F. Martın, and M. Sorolla, "Babinet principle applied to the design of metasurfaces and metamaterials," *Phys. Rev. Lett.*, Vol. 93, 197401, 2004.
13. Xu, H. X., G. M. Wang, M. Q. Qi, and H. Y. Zeng, "Ultra-small single-negative electric metamaterials for electromagnetic coupling reduction of microstrip antenna array," *Opt. Express*, Vol. 20, No. 20, 21968–21976, 2012.
14. Zeng, R., Y. P. Yang, and S. Y. Zhu, "Casimir force between anisotropic single-negative metamaterials," *Phys. Rev. A*, Vol. 87, 063823, 2013.
15. Valagiannopoulos, C. A., N. L. Tsitsas, and A. Lakhtakia, "Giant enhancement of the controllable in-plane anisotropy of biased isotropic noncentrosymmetric materials with epsilon-negative multilayers," *J. Appl. Phys.*, Vol. 121, 063102, 2017.
16. Fu, X. L., G. C. Wu, W. X. Bai, G. M. Wang, and J. G. Liang, "Electromagnetic coupling reduction in dual-band microstrip antenna array using ultra-compact single-negative electric metamaterials for MIMO application," *Chin. Phys. B*, Vol. 26, No. 2, 024101, 2017.
17. Shadrivov, I. V., A. B. Kozyrev, D. W. van der Weide, and Y. S. Kivshar, "Nonlinear magnetic metamaterials," *Opt. Express*, Vol. 16, No. 25, 20266–20271, 2008.
18. Powell, D. A., I. V. Shadrivov, and Y. S. Kivshar, "Nonlinear electric metamaterials," *Appl. Phys. Lett.*, Vol. 95, 084102, 2009.
19. Wang, Z. Y., Y. Luo, L. Peng, J. T. Huangfu, T. Jiang, D. X. Wang, H. S. Chen, and L. X. Ran, "Second-harmonic generation and spectrum modulation by an active nonlinear metamaterial," *Appl. Phys. Lett.*, Vol. 94, 134102, 2009.
20. Wang, Z. Y., Y. Luo, T. Jiang, Z. Wang, J. T. Huangfu, and L. X. Ran, "Harmonic image reconstruction assisted by a nonlinear metmaterial surface," *Phys. Rev. Lett.*, Vol. 106, 047402, 2011.
21. Wall, W. S., S. M. Rudolph, S. K. Hong, and K. L. Morgan, "Broadband switching nonlinear metamaterial," *IEEE Antennas Wireless Propag. Lett.*, Vol. 10, 427–430, 2014.
22. Barbuto, M., F. Bilotti, and A. Toscano, "Power-selectivity horn filtenna loaded with a nonlinear SRR," *9th International Congress on Advanced Electromagnetic Materials in Microwaves and Optics-Metamaterials*, 22–24, Oxford, 2015.
23. Monti, A., M. Barbuto, A. Toscano, and F. Bilotti, "Nonlinear mantle cloaking devices for power-dependent antenna arrays," *IEEE Antennas Wireless Propag. Lett.*, Vol. 16, 1727–1730, 2017.
24. Fernandes, D. E. and M. G. Silveirinha, "Bistability in mushroom-type metamaterials," *J. Appl. Phys.*, Vol. 122, 014303, 2017.
25. Hooper, D. C., A. G. Mark, C. Kuppe, J. T. Collins, P. Fischer, and V. K. Valev, "Strong rotational anisotropies affect nonlinear chiral metamaterials," *Adv. Mater.*, Vol. 29, 1605110, 2017.
26. Lv, W., F. Z. Xie, Y. J. Huang, J. Li, X. C. Fang, A. Rashid, W. R. Zhu, I. D. Rukhlenko, and G. J. Wen, "Nonlinear coupling states study of electromagnetic force actuated plasmonic nonlinear metamaterials," *Opt. Express*, Vol. 26, No. 3, 3211–3220, 2018.
27. Garbic, A. and G. V. Eleftheriades, "Experimental verification of backward-wave radiation from a negative refractive index metamaterial," *J. Appl. Phys.*, Vol. 92, 5930–5935, 2002.